Stiffness study of a robotic system working on vertical building surfaces in Construction field

Elodie PAQUET[a], Balaji GUNASEKAR[a]. Benoit FURET[a], Sébastien GARNIER[a].

[a] University of Nantes, LS2N UMR CNRS 6004, 2 Avenue du Professeur Jean Rouxel, 44475 Carquefou, France
E-mail : elodie.paquet@univ-nantes.fr

Abstract

The paper is devoted to robotic in the construction field based on industrial robotics. The main focus is made on a proper modelling of a robotic system stiffness and identification of their parameters for work on vertical walls. The robotic system is composed of a vertical lift system that can carry a 200kg load including a Doosan cobot (45kg), equipment for tasks to do, and a human operator (80 kg) for working at a height up to 8-10m. Particular attention is paid to the robot's accuracy while working operation (painting, insulation spraying, facade cleaning, etc) and evaluation robot capacity to perform the task with desired precision regardless of the height of the vertical work. In contrast to other works, the robot stiffness is evaluated using a protocol that is based on the deformation of the vertical lift system. The developed approach is applied to find the best geometrical configuration of the scissor lift next to the vertical surface to be worked and the best position of Doosan cobot on the platform lift taking into account the robot working space. The efficiency of the proposed technique robotic solution for the vertical task is validated by experimental study.

Keywords: *Robotic System, Construction robotics, Stiffness model*

1) Introduction

In recent years, the construction field is looking for new ways to perform complex tasks on a large surface in buildings for a task like cleaning and polishing façade as new robotic architecture systems are emerging. Robonaut by NASA was one of the first robots capable of collaborating for space construction applications [1]. Roboclimber is an automated drilling system with a remote-controlled Human interface that is hosted onto a semi-autonomous climbing platform [2]. The reconstruction of buildings, facades, and maintenance tasks can be much more safe, fast, and cheaper with the deployment of robots. Finishing services for productivity improvement on the construction sites were initially studied by Rosenfeld et al. [3], and Warszawski and Rosenfeld [3] [4]. Later, Kahane and Rosenfeld [6] developed a method to assess the effects of human-robot collaboration on automating a construction task and examined the method using an interesting multi-purpose robot, named TAMIR, for block laying and wall painting.

Here, we develop a new robotic architecture proposed and studied to work on vertical walls with a manipulator composed of a cobot Doosan which is a poly-articulated arm fixed on a moving vertical lift mechanism. Doosan M0617 is a cobot with a maximum reach of up to 1700mm and a payload of about 6kg. And also has torque sensors at each joint so that it will be safer for the human operator to share work-space alongside the robot and also prevents damages to the work environment or to the robot itself from collision against wall surfaces. The vertical lift mechanism is commercially more desirable compared to other types of lift mechanisms as it is cheaper and lighter weight, with a greater weight-to-strength ratio. Vertical scissor lifts can support larger weight and move to greater heights. The main objectives of this robotic system (Fig.1) are to reduce working time, get consistent2 quality and free the workers from making dangerous or repetitive tasks

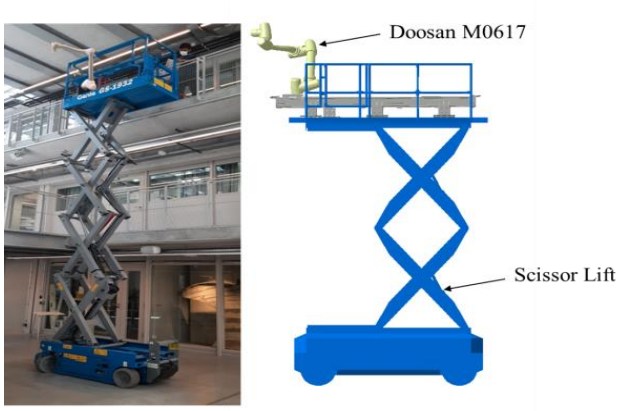

(a)

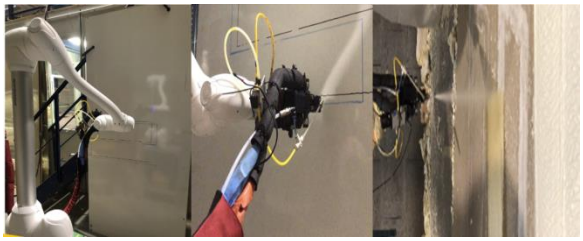

(b)

Fig.1. Developed robotic solution (a), Vertical building Tasks with Doosan (b).

The Doosan robot is positioned on one side of the structure, and counter-weights are employed to return the structure's center of gravity to its original location. The stability of this system is critical to ensuring that the precision of vertical jobs is improved by decreasing stress and position inaccuracy of the end-effector for spraying insulation, as shown in Fig.1. The goal now is to assess the accuracy of the robot's accuracy under stress.

2) Stiffness modeling of robotic system

The positioning of the robot end-effector in the Scissor Lift reference with a set of frames. The positioning of the Tool Center Point (TCP) i.e. R_{Eff} regarding R_{rob} is not considered. Our objective for vertical task focuses on the positioning of R_{rob} regarding R_{Lift}. Therefore, the frames are represented in Fig. 2.

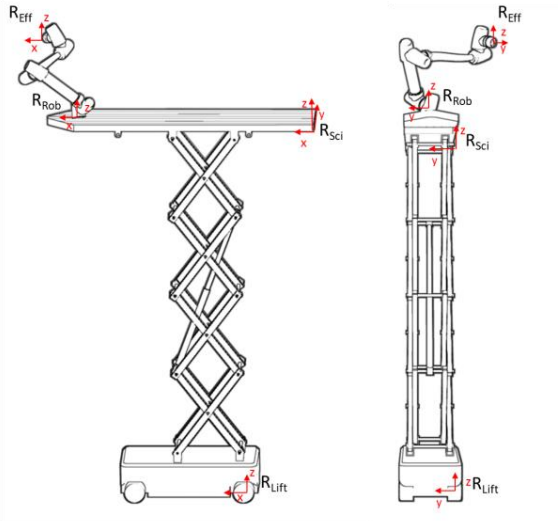

Fig. 2. Positioning of the reference frames

In this section, the stiffness of the scissor lift will be studied with the elements in the fully extended configuration. The vertical force applied by the hydraulic cylinders is very low due to the low slope between the lift's scissor legs. Consequently, the cylinders will have to apply a high amount of force to rise up to escalate to the desired height. Also, the weight distribution in the lift platform may not be always uniform but we assume the weight is uniformly distributed on the lift platform. In our case, we try to analyze the distortion of the GENIE GS-1932 scissor lift using a Laser telemeter.

$$\sigma = F/A$$
$$K = F/U$$

where,

F is force applied (N),
A is the area of cross section (mm^2)
K is Stiffness (N/m)
U is change in Displacement (Position in our case) (m)

$$D = \frac{(n\,(L + W))}{200}$$

where,
D = Maximum allowable platform edge deflection
n = Number of vertically stacked panto-graph leg sections (Scissor Legs)
L = Platform Length
W = Platform Width

Stiffness and Displacement Calculation of Standard Scissor lift (Analytical method):

Beam element with vertical force F_1y and F_2y acting at nodes 1 and 2 with a moment m, rotation ϕ and vertical displacement v.

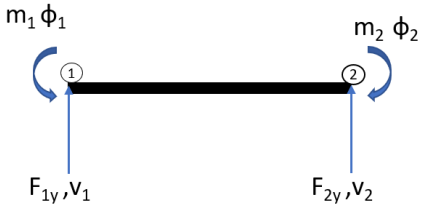

$$\begin{bmatrix} F_{1y} \\ m_1 \\ F_{2y} \\ m_2 \end{bmatrix} = \begin{bmatrix} 12 & 6L & -12 & 6L \\ 6L & 4L^2 & -6L & 2L^2 \\ -12 & -6L & 12 & -6L \\ 6L & 2L^2 & -6L & 4L^2 \end{bmatrix} \begin{bmatrix} v_1 \\ \phi_1 \\ v_2 \\ \phi_2 \end{bmatrix}$$

Table.1.Beam Stiffness Matrix

Frame Element is 2D problem forces along x and y direction of the frame. So along with elastic slope θ_1

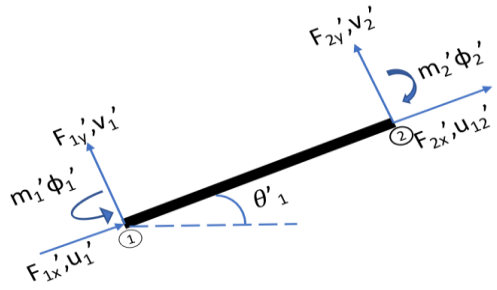

$$\begin{bmatrix} F_{1z} \\ F_{1y} \\ m_1 \\ F_{2z} \\ F_{2y} \\ m_2 \end{bmatrix} = \frac{E}{L} \begin{bmatrix} A & 0 & 0 & -A & 0 & 0 \\ 0 & 12\left(\frac{I}{L^2}\right) & 6\left(\frac{I}{L}\right) & 0 & -12\left(\frac{I}{L^2}\right) & 6\left(\frac{I}{L}\right) \\ 0 & 6\left(\frac{I}{L}\right) & 4 & 0 & -6\left(\frac{I}{L}\right) & 2 \\ -A & 0 & 0 & A & 0 & 0 \\ 0 & -12\left(\frac{I}{L^2}\right) & -6\left(\frac{I}{L}\right) & 0 & 12\left(\frac{I}{L^2}\right) & -6\left(\frac{I}{L}\right) \\ 0 & 6\left(\frac{I}{L}\right) & 2 & 0 & -6L & 4 \end{bmatrix} \begin{bmatrix} u_1 \\ v_1 \\ \phi_1 \\ u_2 \\ v_2 \\ \phi_2 \end{bmatrix}$$

Table.2. Frame Element Stiffness Matrix

Considering the Rotational Matrix while moving from local coordinates to Global Coordinates along x and y direction with rotation around ϕ

$$\begin{bmatrix} u_1' \\ v_1' \\ \phi_1' \\ u_2' \\ v_2' \\ \phi_2' \end{bmatrix} = \begin{bmatrix} cos\theta & sin\theta & 0 & 0 & 0 & 0 \\ -sin\theta & cos\theta & 0 & 0 & 0 & 0 \\ 0 & 0 & 1 & 0 & 0 & 0 \\ 0 & 0 & 0 & cos\theta & sin\theta & 0 \\ 0 & 0 & 0 & -sin\theta & cos\theta & 0 \\ 0 & 0 & 0 & 0 & 0 & 1 \end{bmatrix} \begin{bmatrix} u_1 \\ v_1 \\ \phi_1 \\ u_2 \\ v_2 \\ \phi_2 \end{bmatrix}$$

Table.3. The Global Coordinates Matrix

So, we add the rotation matrix with frame element stiffness matrix:

$$[K] = \frac{E}{L} \begin{bmatrix} Ac^2 + \frac{12Is^2}{L^2} & sc\left(A - \frac{12I}{L}\right) & -\frac{6Is}{L} & -\left(Ac^2 + \frac{12Is^2}{L^2}\right) & -sc\left(A - \frac{12I}{L}\right) & -\frac{6Is}{L} \\ sc\left(A - \frac{12I}{L^3}\right) & As^2 + \frac{12Ic^2}{L^2} & \frac{6Ic}{L} & -sc\left(A - \frac{12I}{L^2}\right) & -\left(As^2 + \frac{12Ic^2}{L^2}\right) & \frac{6Ic}{L} \\ -\frac{6Is}{L} & -\frac{6Ic}{L} & 4I & \frac{6Is}{L} & -\frac{6Ic}{L} & 2I \\ -\left(Ac^2 + \frac{12Is^2}{L^2}\right) & -sc\left(A - \frac{12I}{L^2}\right) & \frac{6Is}{L} & \left(Ac^2 + \frac{12Is^2}{L^2}\right) & sc\left(A - \frac{12I}{L^2}\right) & \frac{6Is}{L} \\ -sc\left(A - \frac{12I}{L^2}\right) & -\left(As^2 + \frac{12Ic^2}{L^2}\right) & -\frac{6Ic}{L} & sc\left(A - \frac{12I}{L^2}\right) & \left(As^2 + \frac{12Ic^2}{L^2}\right) & -\frac{6Ic}{L} \\ -\frac{6Is}{L} & \frac{6Ic}{L} & 2I & \frac{6Is}{L} & -\frac{6Ic}{L} & 4I \end{bmatrix}$$

Table.4. The Global Stiffness Matrix

In addition to the analytical analysis, we analyzed the scissor lifting system with finite element method with elements such as platform and base plate were on the extended configuration for the simulation analysis. The system was fixed in the base platform which was attached to the base plate of the scissor lift. The load acting on the platform is a Uniformly distributed Load of 1000N acting all along the length of the standard scissor platform and 500N point load acting on the extended side of the scissor lift, respectively. These loads were applied vertically on the scissor lift platform to study the system for Stiffness.

Platform Material and Scissor Material

Material	Plain Carbon Steel	Material	6061 Alloy
Yield Strength	$2.20594e+08N/m^2$	Yield Strength	$5.51485e+07N/m^2$
Tensile Strength	$3.99826e+08N/m^2$	Tensile Strength	$1,24084+08N/m^2$
Elastic Modulus	$2.1e+11N/m^2$	Elastic Modulus	$6.9e+10N/m^2$
Poission's ratio	0.28	Poission's ratio	0.33
Mass Density	$7,800kg/m^3$	Mass Density	$2700kg/m^3$
Shear Modulus	$7.9e+10N/m^2$	Shear Modulus	$2.6e+10N/m^2$

Table.5. The characterization for the numerical simulation

The stress distribution and quantity of deformation following mesh creation in each scissor element of the lifting system were studied using numerical simulation. The maximum strain energy hypothesis was used to calculate the system's stress distribution (Von-Mises Stress). On the extended scissor platform, a point load of 500N is operating, and a 1000N evenly distributed load is acting on the remaining scissor platform. The equivalent stress was observed to rise linearly with the applied load on the platform. A scissor lift in extended form with point load (weight of the robot operating on it) demonstrated a maximum Von Mises Stress of 17.63MPa on the system is shown in Figure (3). In planning for design and Model analysis, a minimum stress of around 3.695e-17 Mpa operating on the scissor lift is suggested. The amount of deformation in the components of the scissors lifting system was shown in (Fig:3) owing to point load (p)s, where the center of gravity with no point load is generally the maximum deformation (13.43mm) found at the extended scissor lift platform.

.

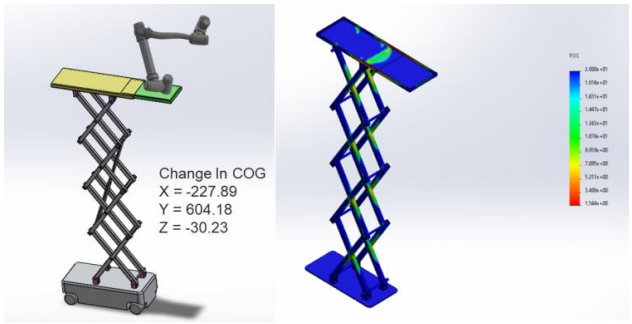

Fig.3. Numerical simulation to analyze the stress distribution and the displacement

Placing a robot on the lift extension platform leads to a change in center of gravity moves 600mm along y-direction and 227mm in x-direction which clearly shows this will lead to tip over criteria or other system failures where the trajectory of the robot must include varying correction factor to maintain good trajectory. With this configuration, we performed the numerical simulation illustrated in figure 4.

The system was considered to be in full functioning height of around 5.4m for this investigation. The center of gravity of the scissor lift changes to x = 64.7mm and y = 2510mm which would result in tipping of the scissor lift, before which the center of gravity is acting on the center of the scissor lift platform was the same for each connection point as shown in Figure 4. This shows the deformation and the COG of the scissor lift. We also see that the deformation results of the scissor lift are closer to that of the Experimental value detailed in the experimental paragraph and this also shows the validation of the structural analysis.

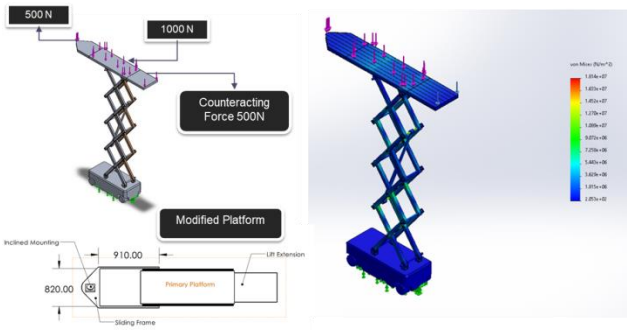

Von mises Stress : Maximum = 1.814 e+07 N/m^2
Minimum = 2.053 e+02 N/m^2

Fig.4. Numerical simulation with another configuration of the Doosan robot

3) Experimental Setup

We design an extended frame setup to mount the Linear Tracker on the Nacelle lift (scissor lift) platform. The standard design of the extended platform frame is fixed onto the Genie GS-1932 with a modified L-joint and screwed rigidly in the hole on the lateral side of the lift. The remaining parts of the extended setup are welded together rigidly except the robot. This extended frame is where the robot will be mounted to work on the vertical wall. Now to understand/study the stiffness of the lift system we use a winch to replicate the payload which would be acting on the real-time in the lift system In the experimental setup, a rope from the winch is hooked onto one end of the lateral rail on the lift platform and pulled using the winch's pulley handle, which is utilized to create the equivalent force (200kg) operating on the lift system in our desired direction. The winch rope is pulled in two directions, one along the platform's y-axis and the other along the z-axis, to generate a dynamic pulling force.

The study is carried on two different wheel configuration of the scissor lift (SL1) and (SL2) at two different heights H_1 = 3m and H_2 =7m along the building floors (Fig.4)

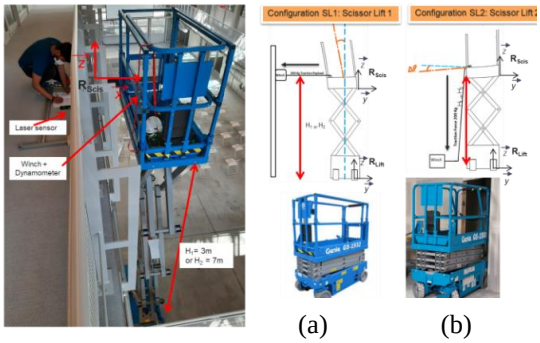

(a) (b)

Fig.5. Experimental setup: Scissor Lift Configurations 1 (a) and Scissor Lift Configurations 2 (b)

The study is carried on two different wheel configuration of the scissor lift at three varying heights along the building floors.

- Wheel aligned along the direction of the mobile platform (Configuration: WC1)
- Wheel aligned at 90◦ steering angle the direction of the mobile platform (Configuration: WC2)

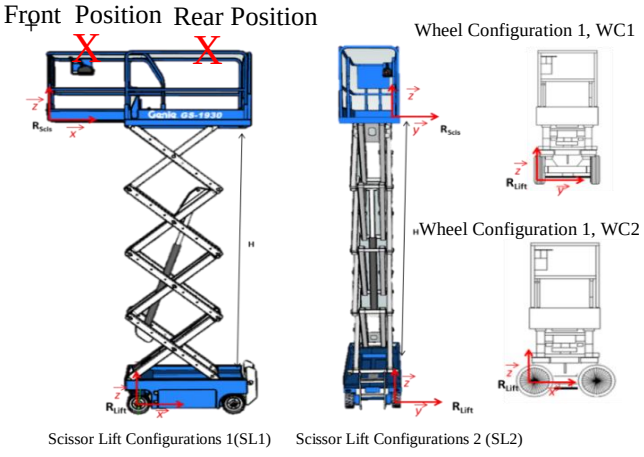

Fig.6. Scissor Lift Configurations (SL1 and SL2) and Wheel Configurations (WC1 and WC2).

For scissor lift configuration 2, wheel configuration 2 at a height of 3m, the stiffness remains high in general throughout the experiment from a minimum force of 88 N to a maximum of 557N. However, for the rear wheel, the stiffness drastically increases in magnitude from 100N/mm to 600N/mm from 295N to 588N.

For scissor lift configuration 2, wheel configuration 1 at a height of 7m, the stiffness remains high in general throughout the experiment from a minimum force of 88 N to a maximum of 557N. However, for the rear wheel, the stiffness drastically increases in magnitude from 100N/mm to 600N/mm from 295N to 588N. For scissor lift configuration 2, wheel configurations 1 and 2, at a height of 7m, the stiffness gradually increases from 20N/mm (front) and 10N/mm (rear) at 80N to 53 N/mm (front and rear) at 588N. Stiffness is almost identical for the front and rear at higher payloads.

Figure 7 shows the displacement and stiffness along the global Y-axis received for configuration 2 measured at two points "Front point" and "Rear point" at two heights 3m and 7m.

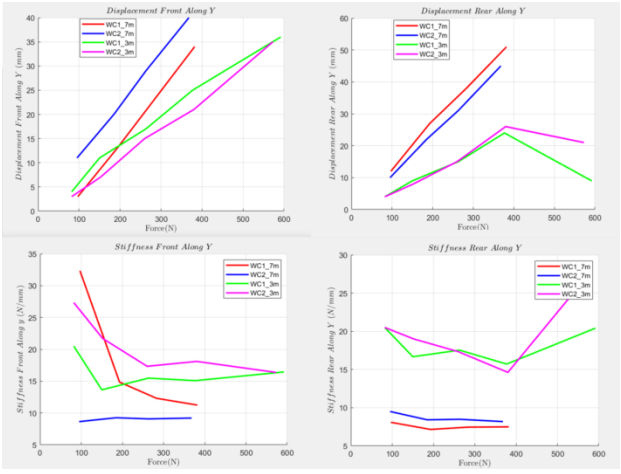

Fig.7.Displacement and Stiffness (Front and Rear) along Y axis:

Figure 8 shows the displacement and stiffness along the global X-axis received for configuration 2 measured at two points "Front point" and "Rear point" at two heights 3m and 7m.

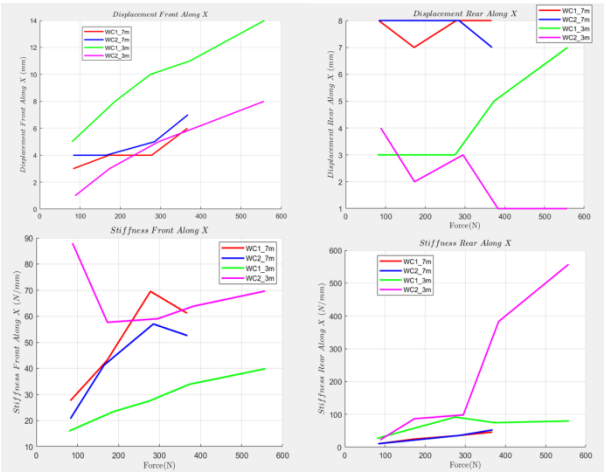

Fig.8. Displacement and Stiffness (Front and Rear) along X axis

When the scissor lift wheel is parallel to the platform, the displacement is large at 3m height in the Y-axis direction in the Front Position, as illustrated in fig. 9. However, at 7m, the x-axis displacement in the Front or Rear positions is relatively minimal.

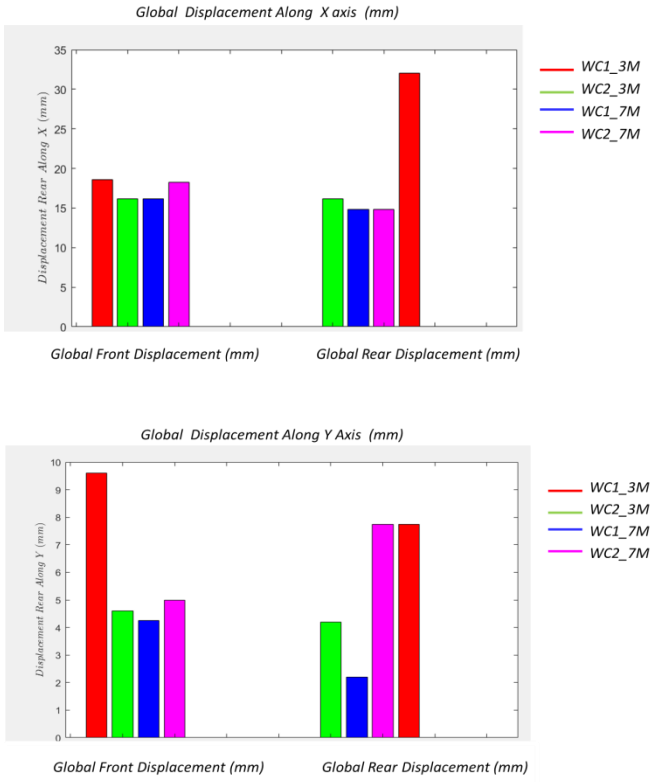

Fig.9. The global displacement of the robotic system in X and Y axis.

4) Conclusions and Perspectives

We offer a new identification approach in this work for a more accurate assessment of the stiffness of a robotic solution for a vertical job. We used a metrological measurement with a physical meaning as the foundation for our approach. For both wheel configurations 1 and 2, the scissor lift configuration 2 offers more rigidity to the system. It increases the stiffness of the system, which results in less displacement. Furthermore, for configuration 2, the system's stiffness values on the back and front sides of the platform are almost similar. As a result, the entire scissor lift will be more isotopically rigid as a result of this. Scissor Lift Configuration 2 as well as any wheel configuration with a fixed robot base would be the optimum solutions for our Task.

The robotic lift system is designed in such a manner that it can accommodate both a robot and a human operator in a collaborative environment, thanks to the optimum platform size.. The deformation and change in the center of gravity of a scissor lift with a robot and a robotics frame arrangement is also investigated, with results that are very close to theoretical and analytical ones.

The stiffness, deformation, and responsiveness of the lift system at various heights and payloads have been calculated, enabling us in determining the optimal configuration for the robotic system. In future study, we will enhance the robot's trajectory planning and optimization to work on complicated wall surfaces in order to fully use the robotic system's workspace on the wall.

5) Acknowledgments

The authors are grateful to Hall6Ouest of Nantes University for provided possibility to carry out experiments with robot Doosan and the Lift Scissor. The work presented in this paper was funded by Nantes University and ROMAS team in LS2N Laboratory, France.

References

[1] M. B. Andrea Bauer, Dirk Wollherr, “Human-robot collaboration: a survey,” International Journal of Humanoid Robotics, vol. 5, no. 1, pp. 47–66, 2008.

[2] M. Z. Rezia M. Molfino∗, Roberto P. Razzoli, “Human-robot collaboration: a survey,” IEEE Robotics and Automation Magazine, vol. 17, no. 2, pp. 111–121, 2008.

[3] A. W. Y. Rosenfeld and U. Zajicek, “Full-scale building with interior finishing robot,” Automation in Construction, vol. 2, no. 3, pp. 229–240, 1993.

[4] e. A. W. Y. Rosenfeld, “Economic analysis of robots employment in building,” 14th International Symposium on Automation and Robotics in Construction, vol. 2, no. 3, pp. 177–184, 1997.

[5] A. W. Y. Rosenfeld and U. Zajicek, “Robot for interior finishing works in building feasibility analysis,” Journal of Construction Engineering and Management, vol. 120, no. 1, pp. 132–151, 1994.

[6] B. Kahane and Y. Rosenfeld, “Balancing human-and-robot integration in building tasks,” Computer-Aided Civil and Infrastructure Engineering,, vol. 19, pp. 393–410, 2004